Topology Design Optimization of Dielectric Substrates for Bandwidth Improvement of a Patch Antenna

Gullu Kiziltas, *Member, IEEE*, Dimitris Psychoudakis, *Student Member, IEEE*, John L. Volakis, *Fellow, IEEE*, and Noboru Kikuchi

***Abstract*—Most literature studies dealing with design optimization for RF applications focused to a large extend on size and shape optimization. So far, material and topology optimization has not been pursued primarily due to the challenges associated with the fabrication of inhomogeneous materials and the limited access to analysis tools. In this paper, we focus on optimum topology/material design of dielectric substrates for bandwidth enhancement of a simple patch antenna. First, the possibility of designing arbitrary dielectric constant materials using off-the-shelf dielectrics is presented as is necessary for the practical fabrication of inhomogeneous substrates. Then, a formal design optimization procedure is conducted using the solid isotropic material with penalization (SIMP) method by relying on a fast full wave finite element-boundary integral (FE-BI) simulator. The SIMP method is a mathematically well-posed topology optimization algorithm because a continuous density function is used to relate the cell variable to the actual material properties. This also allows for a formulation in a versatile optimization framework. sequential linear programming (SLP) is used to solve the nonlinear optimization procedure with the sensitivity analysis based on the adjoint variable method. An important advantage of the proposed design optimization approach is its generality to handle multiple objectives and multidisciplinary problems. Using the proposed automated design procedure, inhomogeneous substrates are designed which allow for 250% bandwidth enhancement of the square patch antenna. Typically, only a few iterations are needed to reach convergence. Finally, the designed substrate is post-processed with image processing and fabricated using thermoplastic green machining.**

***Index Terms*—Broad-band antenna, material design, miniaturization, thermoplastic green machining, topology optimization.**

I. Introduction

IT IS well-known that use of composite materials provides for a greater potential in designing new electromagnetic/RF devices. Recent applications related to the photonic and electromagnetic bandgap structures and ferroelectric material for phase shifter design exist [1]–[3]. So far however, no formal material design procedure has been pursued in the design of volumetric materials for RF applications.

Over the past several years, there has been strong interest in electromagnetic design optimization [4]–[7]. Particular emphasis has been on size and shape optimization rather than material optimization. Shape optimization is certainly more general than size optimization, but nevertheless volumetric design would provide for greater design possibility. To take full advantage of volumetric variations in RF design we need an optimization scheme that can simultaneously select the best geometric and topological configuration while taking into consideration geometry and physical dimensions as well as material composition. Such methods are called topology optimizations. It is reasonable to expect that designs resulting from topology optimization have novel configurations with much higher performance as compared with designs resulting by sizing and shape optimizations, where the topology remains fixed during the design cycle. This paper is aimed at demonstrating that volumetric material design via topology optimization can lead to significant bandwidth improvements in antenna performance.

Topology optimization is regarded as a significant breakthrough in the field of structural optimization. Ever since the seminal paper by Bendsoe and Kikuchi in 1988 [8], this field has expanded significantly, successfully addressing many practical engineering problems [9], [10]. As a result, this method has been widely accepted in industry as a potential design tool [11]. In electromagnetics, there have been a number of recent studies on the topology optimization of electrical devices [12], [13]. However, these have primarily dealt with problem-specific or semi-analytic tools for magneto-static applications. Instead, this paper focuses on a topology design methodology capable of generating novel configurations through the integration of design optimization tools with robust finite element-boundary integral (FE-BI) [14] methods suitable for general EM problems. The latter removes limitations on geometry and material distribution but most importantly it incorporates fast O(N) solvers for rapid solution of large scale problems. Accurate results employing the simulator have already been obtained for scattering and radiation by cavities, slots, and multilayer patch antennas and frequency selective surfaces, demonstrating the method's capability.

The design method used here is the density or solid isotropic material with penalization (SIMP) method [15]. This approach is very attractive to the engineering community because of its simplicity and efficiency. SIMP assumes some explicit relationships between the so-called normalized density ρ and the actual material property, here the dielectric permittivity $\varepsilon = \varepsilon_0 \varepsilon_r$. By dividing the volume into design cells/finite elements a full volumetric design space is introduced. The material property of each

Manuscript received October 8, 2002; revised February 27, 2003. This work was supported by the Defense Advanced Research Projects Agency (DARPA) through a Naval Research Laboratory Grant N00173-01-1-G910.

The authors are with the University of Michigan, Ann Arbor, MI, 48109-2121 USA (e-mail: gkizilta@umich.edu; dpsycho@umich.edu; volakis@umich.edu; kikuchi@umich.edu).

Digital Object Identifier 10.1109/TAP.2003.817539

design cell is controlled simultaneously in each iteration step and updated by following a mathematical algorithm to reach a final design. From this viewpoint, a device is represented by material properties at every point in space via a single density variable.

Since typical electromagnetic problems often require several constraints and numerous variables/design cells, a theoretically well-founded mathematical programming algorithm must be adopted. The sequential linear programming (SLP) [16] is such an algorithm and is adopted here for optimization as opposed to other heuristic optimization algorithms such as genetic algorithms. An essential aspect of the optimization scheme is an evaluation of the EM response (bandwidth) sensitivity to changes in the design variables (dielectric permittivities). Here the adjoint variable method [17] is employed for the sensitivity analysis to enable versatility and fast convergence using first order mathematical programming algorithms.

This paper is structured as follows. First, the potential of designing substrates having pre-specified dielectric properties is explored. We present a practical approach for designing/constructing artificial material volumes by using textures. The verification that arbitrary material constants can be achieved using off-the-shelf materials is essential since it will permit for true material as required by the formal design optimization algorithm using the SIMP method. Validation of the computed effective dielectric constants ($\varepsilon_{\text{reff}}$) of the textured material is carried out by comparing simulation with measurements of the patch resonance frequency. This validation also demonstrates the flexibility of the analysis method to handle high heterogeneous structures. Next (Section III), we extend the application of the SIMP design method to develop substrates with any arbitrary composition subject to antenna bandwidth enhancements. The problem is formulated as a general nonlinear optimization problem and the optimized material distribution is found using the SLP routine together with the sensitivity analysis. Finally, the substrate is fabricated via Thermoplastic Green Machining.

II. Design Practice and Validation

A. Practical Designs Using Textured Materials

Before the formal design optimization approach is considered, we first examine the synthesis of substrates having prespecified dielectric constants. This will provide confidence that any designed ε_r can be synthesized from known material. The proposed electromagnetic (composite) textures (see Fig. 1) are constructed using a mixture of two or more materials so that the resulting dielectric constant ε_r has a predetermined value. A key aspect of the design approach is its practicality. That is, once the mixing formula is mathematically developed, we can then proceed to manufacture it using standard extrusion or machining processes, solid free-form fabrication or rapid prototyping using a linear micro-machining system [18].

The employed textures are motivated from recent studies in the mechanical engineering area employing the design of composites for achieving extremal material properties such as negative Poisson's ratio and negative thermal expansion coefficient, not obtainable by materials found in nature [19]. These designed composites find many useful practical applications such as fasteners and shock absorbers. Similarly, the ultimate goal here is to demonstrate the possibility of obtaining a large dynamic range of dielectric permittivities to possibly guide the construction of optimization models for the desired performance parameters such as bandwidth, isolation and efficiency.

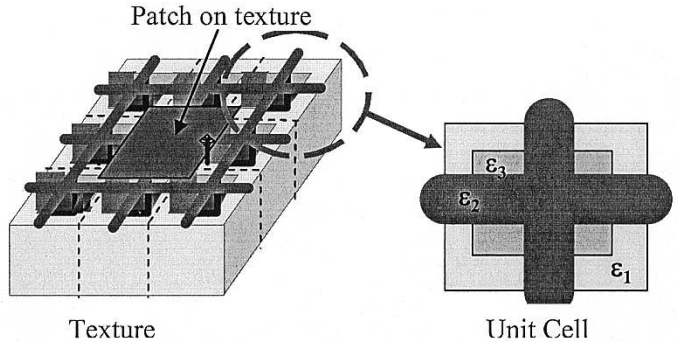

Fig. 1. Illustration of the dielectric substrate (texture) constructed by a 3×3 array of unit cells. Each unit is formed by mixing 3 materials in a prescribed manner.

For our case, the constructed practical textures form the antenna substrate beneath a simple patch as shown in Fig. 1. The designed material/texture is actually constructed by a periodic repetition of a unit cell comprised of a discretized grid of pixels filled with different materials. Each of the material pixels forming the unit cell of the textured material is simply turned on (solid commercial material referred to as low temperature cofiring ceramics (LTCC) or off (air). Alternatively, several material choices can be allowed where each pixel is uniformly filled with one of our choice materials. Fig. 1 shows an example of a unit cell and the resulting texture. The periodicity and pixel by pixel fabrication approach allows for the practical realization of the composite material.

An important aspect of the design process is to design a texture so that its properties represent a pre-specified effective $\varepsilon_{\text{reff}}$. In our analysis, we will determine $\varepsilon_{\text{reff}}$ from the resonance frequency of a simple patch placed on the designed textures. Each of the textures is characterized by a different material composition, be it the type, number, volume composition or topology. However, geometrical parameters such as patch size (1.25 cm $\times$ 1.25 cm) and location (center of textured substrate), dimensions of the textured dielectric substrate ($2.5 \times 2.5 \times 0.0635$ cm) and feed location (center of right edge of patch) all remain unchanged, but do not affect the texture properties.

To design the texture subject to a given $\varepsilon_{\text{reff}}$, the texture characteristics such as the type, number, topology and volume composition of the mixed materials will be varied as required to achieve the pre-specified $\varepsilon_{\text{reff}}$. The process is as follows:

1) Based on the calculated resonance frequency f_r (defined as the frequency where $\text{Im}(Z_{\text{in}}) = 0$), the approximate effective permittivity $\varepsilon_{\text{reff}}$ is found from [20]

$$\varepsilon_{\text{reff}} = \left(\frac{c}{2 \cdot L \cdot f}\right)^2 \tag{1}$$

where c is the speed of light and L is the length of the patch.

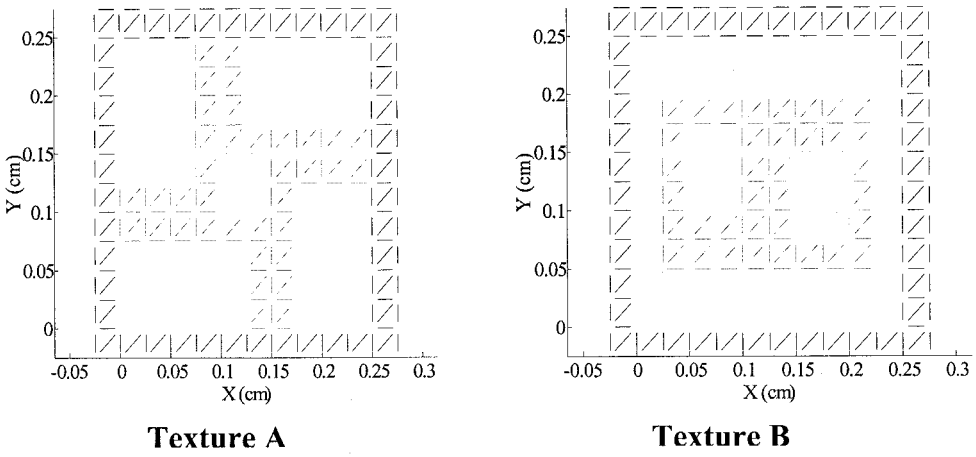

Fig. 2. Example unit cell configuration for the designed textures with two materials: 36% LTCC (shaded) and air (white); textures A and B are only shown; textures C and D (not shown) have the same volumetric composition but differ in topology with A and B. Textures C and D are the same with the only difference in patch location.

TABLE I
EFFECTIVE PERMITTIVITY VALUES FOR DESIGNED TEXTURES WITH TWO MATERIALS (SEE FIG. 2)

Texture Type	ε_r – Mixture formula	ε_r - Resonance based formula
A	36.64	38.3
B		38.3
C		31.25
D		42.87

2) Hammerstad's formula [21], [22] is subsequently used to obtain an updated $\varepsilon_{\text{reff}}$ via (1) taking the fringing length into account.

Alternatively, one could use the mixture formula

$$\varepsilon_{\text{reff}} = \sum_{i=1}^{\text{NM}} \varepsilon_i \cdot V_i \tag{2}$$

for computing $\varepsilon_{\text{reff}}$ (where V_i is the i^{th} pixel volume and ε_i its corresponding relative permittivity). This latter expression is expected to be more and more accurate for finer textures, but in general, it will be shown to primarily provide a guidance rather than a reliable value for general textures.

1) Two Material Mixtures: As a first example of texture design, let us consider a mixture of air and commercial LTCC powder (Bi–Ba–Nd–Ti/BBNT) with $\varepsilon_r = 100$. Of course, many other material combinations are actually possible but these materials were simply chosen for manufacturing and validation purposes. To isolate the effect of texture geometry on the composite's performance, the volume fraction of the LTCC powder is kept constant at 36% (that is, 36% of the texture volume was constrained to LTCC, whereas the remaining 64% was air). The geometries of the textures are selected to obtain the desired permittivity value. A representative designed texture is depicted in Fig. 2. The corresponding $\varepsilon_{\text{reff}}$ values for similar textures are given in Table I. Because of the constant volume percentage between the LTCC and air, the mixture formula gives a constant value of $\varepsilon_{\text{reff}} = 36.64$. However, the value of $\varepsilon_{\text{reff}}$ based on the patch resonance is dependent on the texture and the location of the patch relative to the texture.

More precisely, it is not only the volume composition that matters, as implied by the simple mixture formula, but also the geometry and even the topology in the substrate's performance. Another important observation is that the resulting dielectric constant can be varied by using the same topology (C and D) but different topologies (A and B) can lead to the same $\varepsilon_{\text{reff}}$. The equivalence of the latter and the difference in the former suggest the presence of other characteristics responsible for $\varepsilon_{\text{reff}}$ other than topology alone. In fact, designs C and D possess the same topology, but the patch location relative to the material texture is different. More specifically, the patch is placed on top of the substrate such that its edges coincide with air for texture C and alternating high/low contrast material for texture D, respectively. Consequently, the dominant feature that determines the resonance frequency is the material region that is near the patch edges. Furthermore, the most dominant portion is the part beneath the patch. Another observation is that, the calculated $\varepsilon_{\text{reff}}$ values based on the actual behavior of texture C is lower than the one predicted by the mixture formula. In contrast to the typical expectation that the mixture formula predicts a low bound on $\varepsilon_{\text{reff}}$, texture C demonstrated otherwise. Specifically, we found that textures which have a dominant portion of the low dielectric constant substrate on the boundaries of the patch, predict a lower effective dielectric constant than the mixture formula. This behavior is observed to be consistent with various volumetric compositions and texture scales. We may then conclude that the effective dielectric constant is also affected by the field strength distribution under the patch since the field intensity is higher under the patch region near the edges. Additional designs confirmed this behavior. That is, the location/symmetry of the patch with respect to the texture causes different values for $\varepsilon_{\text{reff}}$.

2) Three-Material Mixtures: The construction of textures using two or more off-the-shelf materials and their electromagnetic behavior is explored in this section. Specifically, a texture is now proposed consisting of three materials: LTCC powder with $\varepsilon_r = 100$, Diopside (Ca–Mg–Si–O) with $\varepsilon_r = 10$ and air. The volume fraction of the powders is varied this time

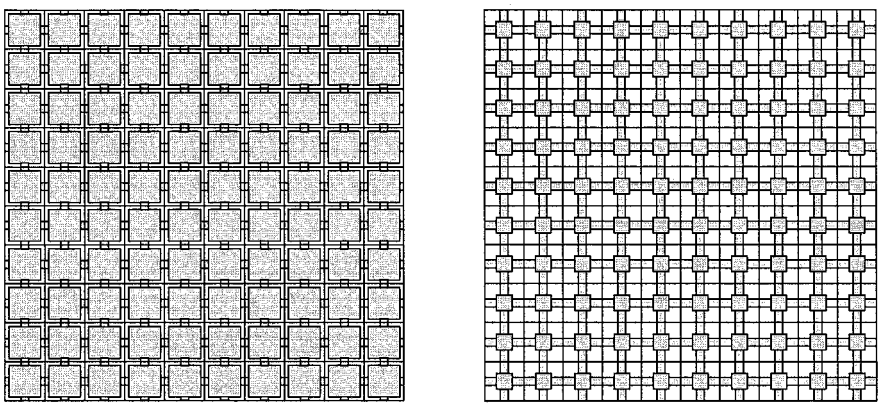

Fig. 3. Examples with different mix of materials but the same topology.

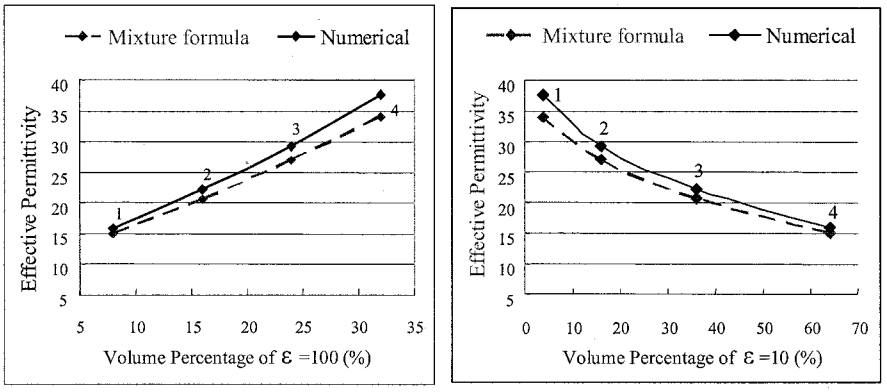

Fig. 4. Effective dielectric permittivity variation of the designed three material textures with respect to the volume composition of $\varepsilon = 100$ and $\varepsilon = 10$ material comprising the texture.

but the topology of the textures is kept constant and resembles a square-cross texture. The geometries of the textures are again finalized subject to the desired permittivity value (see Fig. 3). Example curves of the effective permittivity value as a function of the volume composition is shown in Fig. 4. The importance of these curves is that the same topology but different material percentages can lead to large dynamic ranges in the attainable values for $\varepsilon_{\text{reff}}$. Thus, we are confident that the mixture of off-the-shelf materials leads to a large range of $\varepsilon_{\text{reff}}$, and this characterization needs to be considered for designing RF devices that exploit both geometry and material. Before proceeding with the design of a specific antenna, where the material rather than its shape is varied, we first carry out a simple validation of our $\varepsilon_{\text{reff}}$ computations given above. Of particular interest is the validation of the analysis for the textured dielectrics of high contrast materials.

B. Validation

For validation purposes, an LTCC substrate ($\varepsilon = 100$) is manufactured using the Micro- Fabrication with Co-Extrusion (MFCX) technique [23]. This technique can produce any design with axial symmetry from several different materials starting with materials in powder form. More precisely, LTCC is originally in powder form and undergoes specific solidification processes to meet specified material characteristics according to warehouse guidelines. First, a thermoplastic compound is prepared by mixing the LTCC powder with specific polymer binder systems. This is actually a two-step process where the ceramic powder is ball milled and then shear mixed with binder systems under specific conditions. Once compounded, it is warm pressed and the dielectric block in its "green body" solid state is obtained. At this stage, complicated designs with features as fine as 10–100 μm are constructed by a repeating process of size reduction thru co-extrusion and reassembly. After co-extrusion, the final step is to remove the polymer with a binder burnout process that densifies the resulting ceramic material via a co-firing process. Both processes comply with specific temperature and time requirements. If processed according to the specific material guidelines, the expected substrate properties are $\varepsilon_r = 95 \pm 5$ with a loss tangent less than 0.05% at 1 MHz. It is noted that the LTCC material is also specified to be frequency independent with less than 10% variation in the frequency range of interest.

The final produced substrate for measurement purposes is an LTCC ($\varepsilon = 100$) texture consisting of a 5×5 array of square holes embedded in the LTCC material (see Fig. 6). In addition, to attain a smooth surface, the holes were filled with stycast®W19 with $\varepsilon_r = 3.3$. To obtain the resonance frequency and $\varepsilon_{\text{reff}}$ of the textured material, a square 1.4 cm $\times$ 1.4 cm metallic patch is painted on top using ECCOCOAT® C-110–5 silver paint. A microstrip aperture feed is then used to excite the patch as shown in Fig. 6. The aperture feed uses a RT/Duroid 6010 substrate with $\varepsilon_r = 10$ and thickness 0.254 cm and the details are given in Fig. 5. The microstrip has a width of 0.3 cm and

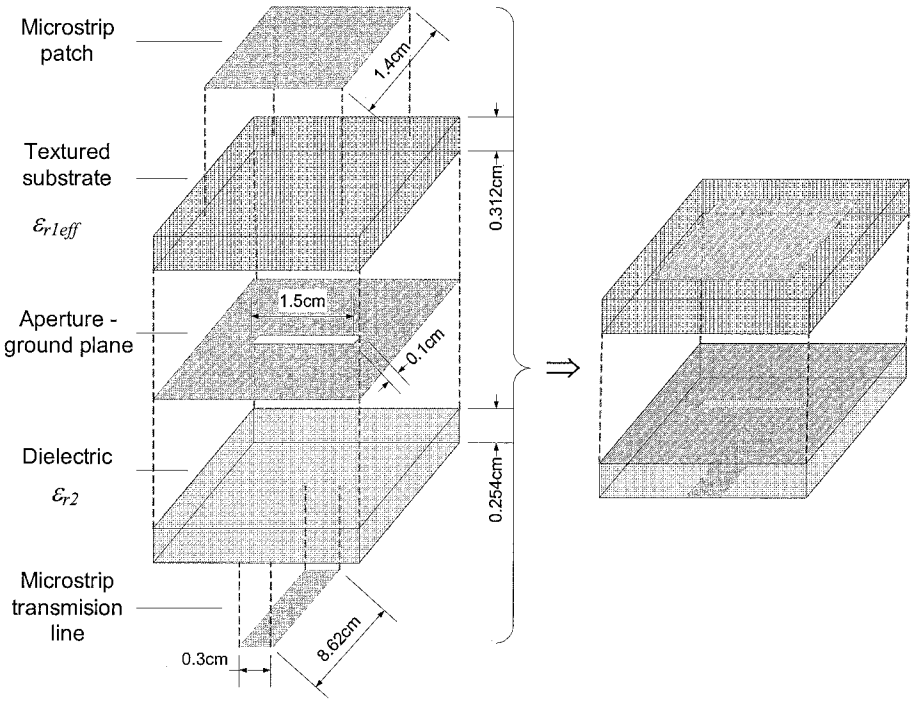

Fig. 5. Schematic for the microstrip antenna and aperture feed design.

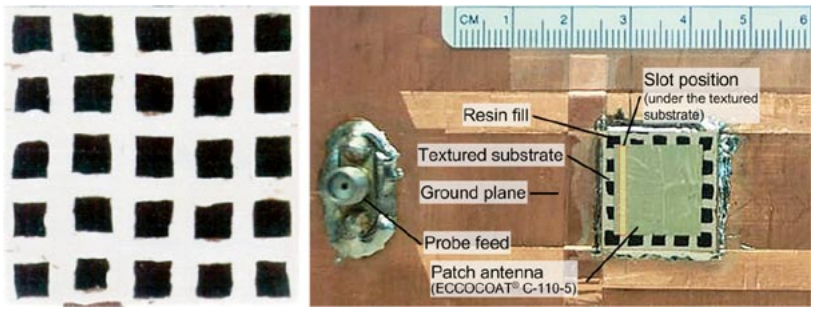

(a) (b)

Fig. 6. (a) Textured substrate and (b) microstrip antenna and feed configuration.

length of 8.62 cm chosen to obtain a characteristic impedance of 50 Ω and a length of 1 λ at 1 GHz. Also as displayed, the aperture slot is located on the ground plane of the microstrip at a distance 2.1 cm away from the microstrip termination. The slot is perpendicular to the microstrip and has dimensions 1 mm by 15 mm (see Fig. 5). Finally, the microstrip is fed using a probe positioned at the end away from the slot. The overall fabricated piece is depicted in Fig. 6 with the textured substrate shown in (a).

As mentioned earlier, prior to printing the patch, the material undergoes binder burn-out and sintering processes. This amounts to generating the appropriate microstructure on the scale of the crystal grains and domains without residual porosity. A challenge during the co-sintering is that the temperature-time history must be near-optimal for both phases [23]. Otherwise, cracking may occur. It is also understood that the materials must have similar thermal expansion coefficients, to prevent the build up of thermal mismatch strains during cooling. For these reasons and more importantly due to imperfections during coextrusion, the process led to a slightly distorted texture (see Fig. 6).

The measured and computed resonance frequency for the structure shown in is 1.357 GHz and 1.359 GHz, respectively (with a typical bandwidth of 3%). The typical return loss and gain graphs are omitted for space reduction. It is remarked that the resonance location implies an $\varepsilon_{\text{reff}} = 63$ leading to a miniaturization of 4 as compared to using $\varepsilon_r = 4$. More importantly, a gain of 6.7 dBi was measured, which verifies the assumption of a lossless substrate in our design

In the next section, we proceed with the integration of analysis and design methods and its use in an RF design problem. The specific design example pursued is the design problem of a textured substrate subject to certain pre-specified bandwidth requirements.

III. Design Optimization of a 3-D Material Substrate

A. Design Methodology

The design algorithm adopted here is based on the density/SIMP method. In the context of SIMP, the material property depends on some power of the artificial variable density ρ,

where ρ is introduced and related to the actual dielectric constant. As is well known, solution of topology optimization problems using mathematical programming algorithms is only possible with continuous design variables. Thus, a scheme is required for specifying a material whose properties taper from say $\varepsilon_r = 100$ ($\rho = 1$) to air ($\rho = 0$). Actually, the most straightforward image-based geometry representation is the "0/1" integer choice, where the design domain is represented by either a void or a filled/ solid material variable and this was adopted in [6]. This is also known as the "black and white" design. However, this formulation is not well-posed mathematically. It can be converted into a well-posed one by incorporating microstructures into the extended design domain to allow for materials with intermediate properties; that is, materials having graded properties [12]. This is the essence of the density method in which material grading is achieved using a single continuous variable, ρ, to represent the material property of each finite element/pixel in the design domain. The approach has the advantage that a material property is interpolated/graded using a smooth continuous function, which only depends on a single material density variable and almost all possible topologies can be designed within the resolution of the finite element discretization. A suitable interpolation of the dielectric permittivity also known as the density function is

$$\rho = \left[\frac{(\varepsilon_{\text{int}} - \varepsilon_{\text{air}})}{(\varepsilon_{\text{orig}} - \varepsilon_{\text{air}})}\right]^{1/n} \tag{3}$$

where ε_{int} and $\varepsilon_{\text{orig}}$ are the intermediate and available original (relative) dielectric permittivities of the solid, respectively. The power $1/\text{n}$ is an empirical penalization power smaller than 1/2 for convergence purposes [8].

Using the density method, a general nonlinear optimization problem is formulated and solved by a SLP method [16]. SLP is capable of handling a large number of design variables but any other gradient-based optimization algorithm could be used. The sensitivities are calculated by the adjoint variable method. The latter method not only provides for efficient computation of the sensitivities necessary for optimizing the electromagnetic performance merits, but also facilitates the interface with the FE model. The actual optimization procedure is described in the next section. We then proceed with a specific bandwidth optimization example.

B. Optimization Model

The general nonlinear optimization problem to be solved is mathematically defined as: Find the set of variables $\vec{x}$ that will minimize the function

$$f(\vec{x}) \tag{4}$$

$$\text{Subject to} \quad h(\vec{x}) = 0, \quad g(\vec{x}) \leq 0 \tag{5}$$

$$\text{and the constraints:} \quad x_i^l \leq x_i \leq x_i^u, \quad i = 1, N \tag{6}$$

where $\text{f}(\vec{x})$ is the objective function, $\text{h}(\vec{x})$ is the equality constraint, $\vec{x}$ is the vector of design variables. Also, $\text{x}_k{}^l$ and $\text{x}_k{}^u$ are the lower and upper bounds on the N design variables, respectively.

The goal for the electromagnetic topology design considered here is to maximize the bandwidth of a patch antenna by altering the distribution of the dielectric permittivity of its substrate. A suitable optimization model is

$$\text{Minimize} \quad \left[\max(|s_{11}|_j)\right] \; j = 1, \ldots N_{\text{freq}} \tag{7}$$

$$\text{Subject to} \quad \sum_{i=1}^{\text{NFE}} \rho_i \cdot V_i \leq V^* \tag{8}$$

$$\text{with side constraints}: 0 < \rho_{\min} \leq \rho_i \leq \rho_{\max}, \; i = 1, ..NFE \tag{9}$$

$$\text{where} \quad |s_{11}|_j = \frac{\left|Z_{\text{in}_j} - Z_0\right|}{\left|Z_{\text{in}_j} + Z_0\right|}(\text{dB}) \tag{10}$$

refers to the return loss at the j^{th} sampling frequency, Z_{in_j} is the input impedance at the feed at the same frequency, Z_0 is the reference impedance and NFE refers to the number of cells/finite elements within the domain. By minimizing the highest return loss among the N_{freq} samples, we could reduce the difference between the highest and lowest $|s_{11}|$ and thus achieve a larger bandwidth [4]. It is noted that the actual problem solved is the dual of the above problem (7)–(10). The dual of the problem is known to yield the same exact solution and corresponds to a standard minimization problem with a modified objective function and added constraints as follows:

$$\min X \tag{11}$$

$$|s_{11}|_j \leq X \quad j = 1, \ldots N_{\text{freq}}. \tag{12}$$

In the above, X is an additional design variable in the solution process. Other constraints (8)–(10) are retained in the optimization model. In fact, the constraint (8) poses a requirement on the total volume expressed in terms of volume (V_i) and density (ρ_i) of the material pixels comprising the substrate. The volume constraint is necessary for several reasons. First, it is known to guide the design process toward a black and white design to make "efficient" use of the available material for specific problems [29]. More specifically, if there is no volume constraint, intermediate density areas will just be as "economical" as full density areas and a grey scale design is more likely to occur. The volume constraint is also imposed as an upper bound on the approximate effective permittivity, hence a lower bound on the resonance frequency of the patch printed on the synthesized material. This in turn correlates the initial bandwidth and the final optimized bandwidth by simply eliminating the trivial solution of bandwidth enhancement via a lower dielectric constant. Another well-known mathematical reason for the volume constraint is the requirement for mathematical convergence. More specifically, as in any nonlinear optimization problem, to converge to a feasible solution (or feasible optimum), the design space must be closed-bounded. In that respect, the presence of a volume constraint gives boundedness and ensures mathematical convergence. Finally, the side constraints (11) impose lower and upper limits on the relative densities of each design cell with $\rho_{\min}$ being the lower bound vector and $\rho_{\max}$ being the corresponding max value. In this manner, the actual material distribution within the substrate stays within predefined bounds.

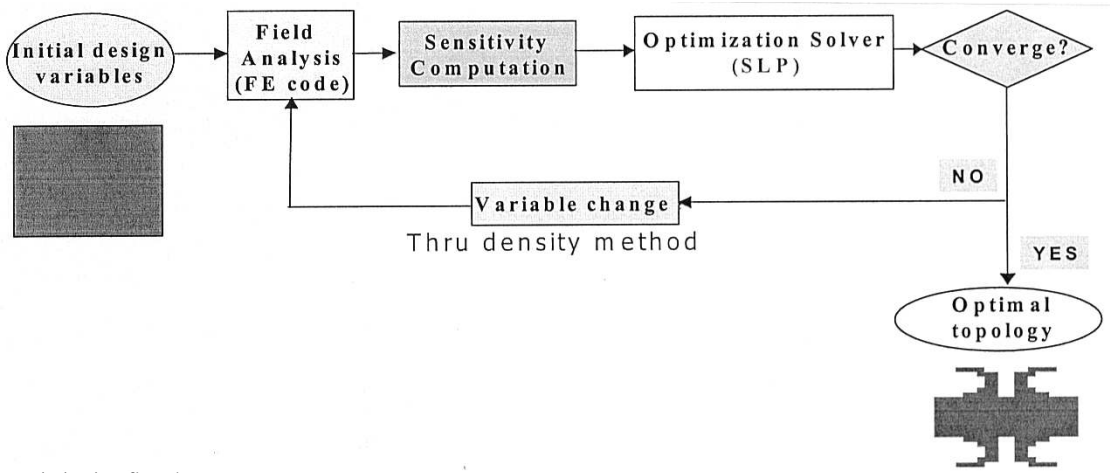

Fig. 7. Design optimization flowchart.

C. Numerical Implementation

The optimization statements (8)–(12) are nonlinear and must be satisfied by an iterative procedure where a linear subproblem is solved at each step. Examples of such algorithms are the SLP, like the CONLIN [24] and DSPLP [25] routines or the method of moving asymptotes (MMA) [26]. The iterative optimization scheme used here is the SLP method employing the package DSPLP in the SLATEC library [25] for the numerical implementation of the optimization problem. This method was found reliable and quite efficient. In each optimization iteration, the objective function and constraints are replaced by linear approximations obtained from the Taylor series expansion about the current design point $\vec{x} = \{\vec{\rho}\}$. The linear programming subproblem is then posed to find optimal design changes $\Delta\vec{x}$ from the current design point. This can be mathematically stated as:

Minimize the linearized objective function

$$f(\vec{x}^{\langle k\rangle}) + \sum_{i=1}^{Ndv} (\Delta x_i) \left(\frac{\partial f}{\partial x_i}\right)\Big|_{x^{\langle k\rangle}} \tag{13}$$

for Ndv design variables

$$\Delta\vec{x} = \vec{x}^{\langle k+1\rangle} - \vec{x}^{\langle k\rangle} \tag{14}$$

subject to the linearized volume (V) constraint

$$V_{\min}{}^{(m)} - V^{(m)}\left(x^{\langle k\rangle}\right) \le \sum_{i=1}^{Ndv} \Delta x_i \left(\frac{\partial V^{(m)}}{\partial x_i}\right)\Big|_{x^{\langle k\rangle}} \le V_{\max}{}^{(m)} - V^{(m)}\left(x^{\langle k\rangle}\right) \tag{15}$$

other linearized constraints g

$$g_j{}^{\min} - g_j\left(x^{\langle k\rangle}\right) \le \sum_{i=1}^{Ndv} \Delta x_i \left(\frac{\partial g}{\partial x_i}\right)\Big|_{x^{\langle k\rangle}} \tag{16}$$

$$\text{and} \quad (\Delta x_i)_{\min} \le (\Delta x_i) \le (\Delta x_i)_{\max}. \tag{17}$$

The last set of constraints (17) stand for move limits, with $(\Delta x_i)_{\min}$ and $(\Delta x_i)_{\max}$ being the lower and upper bounds on the allowable change in the design variable. The move limit bounds are important since the optimization iteration may never converge without their proper choice. Typically, during one iteration, the design variables are allowed to change by 5%–15% of their original values.

After optimization of one subproblem, a new set of design variables, $\vec{x}^{\langle k+1\rangle} = \vec{x}^{\langle k\rangle} + \Delta\vec{x}$ is obtained and updated in each design cell/finite element. As a result, the design domain has a new topology with an effective dielectric permittivity yielding a performance closer to the specified targets. The iterations proceed until convergence in the objective function is achieved. Substantial computational time can be, of course, saved if the starting guess is close to the optimal topology. Thus, as a rule, we begin with a rough pixel/coarse mesh design. The design domain is subsequently divided into finer elements to form a refined model used as the starting guess in the subsequent optimization steps.

D. Computational Procedure

The procedure is initiated by specifying several design parameters: patch geometry and the material characterization, i.e., the dielectric block dimensions and initial homogeneous dielectric constant. Also, the feed location and amplitude, and the frequency range of operation are specified. Afterwards, the design domain is discretized into a large number of finite elements and the available material is distributed throughout the domain usually as a homogenous substrate. At each iteration, the following three steps are executed: 1) prior to starting the iteration solve the finite element problem using the FE-BI solver; 2) perform a sensitivity analysis involving the numerical solution of an additional set of finite element system equations; 3) pursue an optimal material redistribution based on the SLP-scheme.

Convergence of the above procedure is achieved when the changes in the objective function and design variables from iteration to iteration get below a certain value (typically 10^{-3}). One can actually get a general form of the final topology in less than 50 iterations, depending on the number of elements and constraints and the complexity of the design domain. The whole design process may take from a few minutes to several hours on a modern workstation (500 MHz to 1 GHz processors). A flowchart of the optimization algorithm demonstrating the steps described here is given in Fig. 7.

The actual design algorithm is a custom-made code written in FORTRAN90. A simple in-data file allows for simplified entering of the design problem, material data and constraints. A separate user-interface is then used to interface the FE-BI solver with the optimization routine. Graphical outputs showing input impedance and return loss as a function of frequency and material distribution outputs after convergence via the SDRC IDEAS CAD package are possible.

E. Sensitivity Analysis

The problem linearization (mentioned earlier) at each iteration requires the knowledge of the gradients (sensitivities) of the objective function and constraints relative to the design variables. In other words, the derivatives of the electromagnetic response function, the return loss for our case must be determined as a function of the design variables. Needless to mention, the sensitivity analysis is of pivotal importance in solving any gradient-based optimization problem. The derivation and implementation are briefly discussed here for the return loss function and are based on the discrete form of the adjoint variable method. That is, the finite element formulation is used to carry out analytical differentiation because of its computational efficiency and high accuracy. Other required differentiations are explicit derivatives and won't be discussed. To start with, we introduce the objective function $|s_{11}|$ functional of

$$|s_{11}| = f(\mathrm{E}(\varepsilon(\rho)), \varepsilon(\rho)) \tag{18}$$

where ε refers to the element dielectric permittivity assumed to be lossless, ρ denotes the element density as defined earlier, and E are the electric field edge unknowns in the hybrid FE-BI formulation and result from a solution of

$$[A]\ \{E\} = \{f\}. \tag{19}$$

Noting that all variables are complex except ε and ρ, and on applying the chain rule of differentiation twice together with the approximation for the derivative of the real variable $|s_{11}|$ [27] in (18), the following sensitivity expression is generated:

$$\frac{d|s_{11}|}{d\rho} = \left\{ \frac{\partial |s_{11}|}{\partial \mathrm{Re}(s_{11})} \mathrm{Re}\left[\frac{\partial s_{11}}{\partial \varepsilon}\right] + \frac{\partial |s_{11}|}{\partial \mathrm{Im}(s_{11})} \mathrm{Im}\left[\frac{\partial s_{11}}{\partial \varepsilon}\right] \right\} \frac{\partial \varepsilon}{\partial \rho}. \tag{20}$$

All terms in (20) are easily calculated by explicit differentiation but to find $\partial s_{11}/\partial \varepsilon$, we must apply chain rule to obtain

$$\frac{\partial s_{11}}{\partial \varepsilon} = \frac{\partial s_{11}}{\partial E} \frac{\partial E}{\partial \varepsilon}. \tag{21}$$

This result requires the evaluation of $\partial E/\partial \varepsilon$, viz. the differentiation of the FE-BI generated fields (19) given by

$$\frac{\partial E}{\partial \varepsilon} = [A]^{-1} \left(\frac{\partial f}{\partial \varepsilon} - \frac{\partial [A]}{\partial \varepsilon} E \right). \tag{22}$$

Substituting this into (21) gives

$$\frac{\partial s_{11}}{\partial \varepsilon} = \frac{\partial s_{11}}{\partial E} [A]^{-1} \left(\frac{\partial f}{\partial \varepsilon} - \frac{\partial [A]}{\partial \varepsilon} E \right). \tag{23}$$

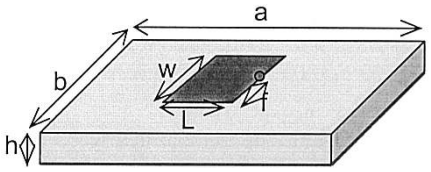

Fig. 8. Sketch of the patch antenna with initial homogenous dielectric substrate.

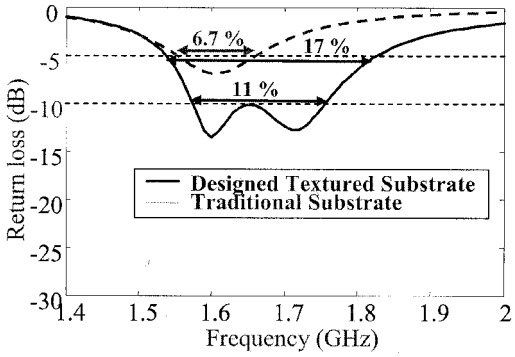

Fig. 9. Return loss for the cavity backed patch when situated on a homogenous (traditional) and optimally designed textured substrate.

Obviously, the calculation of the first term in the expression (23)

$$\lambda = \frac{\partial s_{11}}{\partial E} [A]^{-1} \tag{24}$$

requires the inversion of matrix [A] for each design variable per iteration. This is computationally expensive and most likely not practical. Thus, we instead solve the system

$$\lambda^T = \left([A]^{-1}\right)^T \left(\frac{\partial s_{11}}{\partial E}\right)^T \tag{25}$$

which is easily recognized as the transpose solution (adjoint variable [27]) of the original FE-BI matrix system. Due to symmetric nature of [A] we rewrite (25) as

$$\lambda^T = [A]^{-1} \left\{\frac{\partial s_{11}}{\partial E}\right\}^T \Rightarrow \quad [A]\ \{\lambda\}^T = \left\{\frac{\partial s_{11}}{\partial E}\right\}^T \qquad [A]\ \{E\} = \{f\} \tag{26}$$

and, thus, an iterative solution of the latter gives $\{\lambda\}$. It should be noted that the embedded term $\partial [A]/\partial \varepsilon$ is computed on the local element level and this allows for substantial CPU savings since only the local element matrices need be differentiated. The final sensitivities $d|s_{11}|/d\rho$ at each element are obtained by solving the adjoint problem of the finite element formulation (26) and utilizing (23) in (20) for each sampling frequency point at each iteration.

IV. Bandwidth Enhancement Design Example

To summarize, the outlined design procedure involves several algorithms and related interface modules. Of these, the EM algorithm generality and CPU speed as well as the robustness of the sensitivity analysis are crucial to obtaining a good design. In this section we demonstrate the capability of the procedure by carrying out an antenna design problem. Since the focus is on materials design, a sample patch antenna is considered. More precisely, patch antennas (see Fig. 8) are known for their narrow

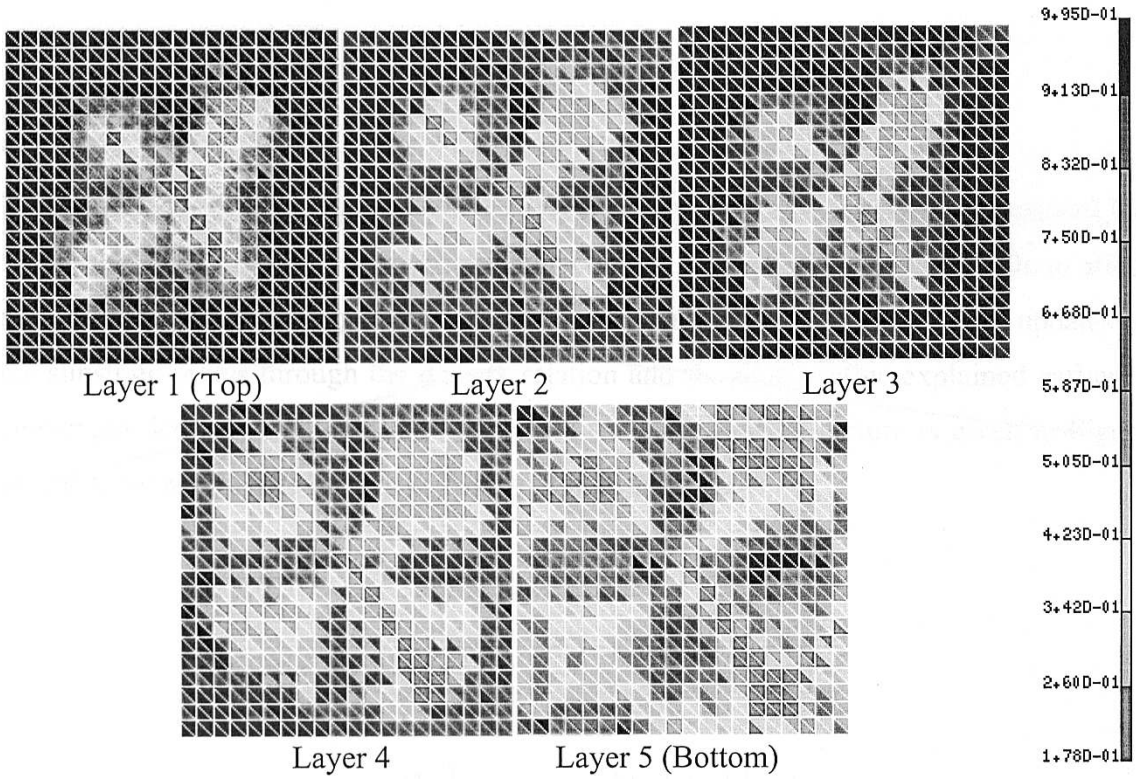

Fig. 10. Optimally designed textured density (material) distribution for each layer of the substrate supporting a patch (layers counted from top). The grey-scale (right) presents the density variable.

bandwidth [28], which is reduced further when high contrast dielectric materials are used for miniaturization purposes. Consequently, a suitable challenging design optimization problem is that of increasing a fixed size patch antenna bandwidth through substrate material design.

The antenna dimensions are depicted in Fig. 8 and for our design, we choose a domain comprised of $\mathrm{NFE} = 4000$ (20*20*2*5) finite elements. The square patch ($\mathrm{W} = \mathrm{L} = 1.25\ \mathrm{cm}$) is located at the center of the substrate's top surface with dimensions $\mathrm{a} = \mathrm{b} = 2.5\ \mathrm{cm}$ and thickness $\mathrm{h} = 3.175\ \mathrm{cm}$ (W, L and h are fixed). A probe feed is selected and placed at $\mathrm{d} = 0.625$ distance from the right lower corner of the patch. Bandwidth enhancement is expected to occur near the resonance of the initial structure. Therefore, 21 frequency points ($\mathrm{N_{freq}}$) are used to sample across 1–2 GHz frequency range (the expected range where patch resonance will occur). Special emphasis is placed on setting the volume constraint to ensure a higher value for the resulting optimized effective dielectric constant to achieve better miniaturization with respect to the initial dielectric constant of the substrate. This is necessary to prevent a trivial solution to bandwidth improvement. To evaluate bandwidth (and VSWR) it is necessary to set the reference input impedance $\mathrm{Z_0}$ and we chose the usual value of 50 Ω. Also, for this design the material will be assumed to be lossless. The optimized effective permittivity is obtained by using a suitable texture of the LTCC material with $\varepsilon_r = 100$ and a volume constraint of 70% of the design domain. It is noted that the initial substrate with $\varepsilon_{\mathrm{int}} = 42$ corresponds to a density $\rho = 0.65$ value for each design pixel with a penalization factor of $\mathrm{n} = 2$ via the density function (3). This

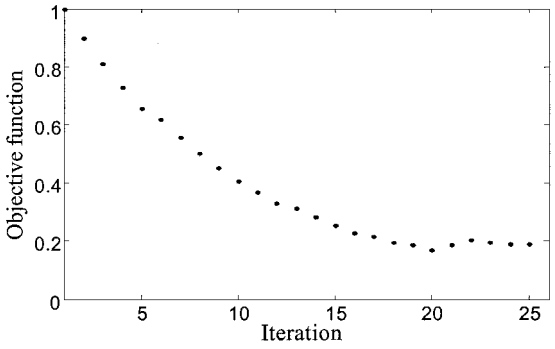

Fig. 11. Objective function convergence history for the example design in Figs. 10 and 11.

in turn, implies that the volume constraint (10) is satisfied for a uniform discretized mesh corresponding to the same volume V_i for each design cell. In other words, the initial design with $\varepsilon_{\mathrm{int}} = 42$ and $\rho = 0.65$ corresponds to 65% occupation of the whole design domain with the solid LTCC material.

The initial homogenous substrate delivered a 5 dB return loss bandwidth of 6.7% shown by the dashed curve in Fig. 9. However, typically the 10 dB bandwidth is quoted but because of the capacitive nature of the high contrast substrate, we were not able to attain a 10 dB bandwidth. In proceeding with the optimization process to carry out updates of the substrate pixels through the density relation and the SLP routine explained earlier, a converged design was obtained in 20 iterations. The resulting texture is given in Fig. 10 and the convergence history is displayed in Fig. 11.

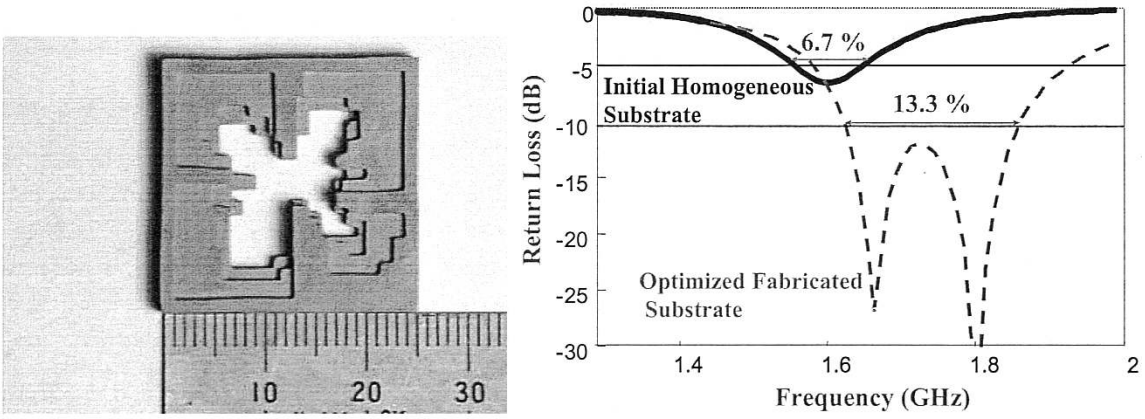

(a) (b)

Fig. 12. (a) Fabricated substrate after filtering and modifications and its return loss performance comparison with (b) initial homogenous substrate.

The achieved impedance and return loss of the optimal design shows a 10 dB bandwidth of 17% as predicted by the solid curve in Fig. 9. The computation for each iteration required 2.5 min/freq, i.e 52.5 min for the whole frequency range on a Pentium 3.0. Given the poor bandwidth at the starting point of the design, the attained bandwidth performance is truly remarkable. Moreover, further bandwidth improvement is possible via patch shape design. Also, a consideration of competing tradeoffs between patch size or bandwidth and the value of ε_r is possible. In addition, use of magnetic materials offer additional possibilities. The optimized material distribution is actually a 3-D color coded block because the substrate was modeled in FEM using five layers. Fig. 10 shows the density (material) distribution across each layer and corresponding density scale. The grey-scale corresponds to the density variable in (3), which is analogous to the dielectric constant. Because of the grey scale distribution, the resulting design is not easily manufacturable and to do so we need to re-digitize the material to a few values of ε_r. This can be done through a restriction/penalization process or via image processing/filtering techniques. The former is realized through some sort of global or local mathematical restrictions on the density function variation and is imposed on the original formulation of the topology optimization problem. Although not proven successful for classical problems, each presents issues with regard to solution existence and implementation difficulty. The alternative of image processing is simpler and is based on the idea of substituting the closest solid material to manufacture each design cell. If combined with manual intervention, it has been shown to result in successful practical designs and has been therefore extensively used. Consequently, to fabricate the design, we applied post processing/image processing techniques to transform the initially obtained substrate design into a two material (available material) composite. More specifically, the simple filtering idea based on a cutoff value of 0.64 for the densities was adapted to solidify and fabricate the 3-D material substrate. Thermoplastic Green Machining is then used for fabrication. This process is similar to the MFCX discussed in Section II.B, except that coextrusion is replaced by conventional drilling.

More specifically, a thermoplastic compound is first prepared and solidified. The material is machinable at the "green body" state and at this stage it has slightly larger block dimensions than the original desired design. After removing material via a computer-controlled drilling machine (Modela; Roland DG Corporation, Japan) in accordance to the filtered design geometry, this substrate undergoes binder burn out and sintering processes as earlier. During machining, the design is also slightly modified for machinability with consideration for shrinkage after sintering. The fabricated substrate is depicted in Fig. 12(a). The return loss behavior of the final fabricated design is compared to the initial substrate [see Fig. 12(b)]. It is important to note that the attained bandwidth was even further improved for the fabricated design. This demonstrates the advantage of integrating robust optimization techniques with simple filtering processes for practical manufacturable substrates with improved performance.

V. Conclusion

The aim of this study was to explore the possibility of designing new substrate textures and topologies for performance improvements in electromagnetic applications. Our approach was based on mixing off-the-shelf commercial LTCC, Diopside and air at several levels of granularity to different type of textured unit cells that exhibit new RF properties. First, it was demonstrated that different mixtures and textures of available materials can be used to emulate a large dynamic range of ε_r values. Simulations were used to verify the dielectric constant of the resulting texture and a measurement of such a texture was included to validate the design. Having established the means of emulating different material properties from available LTCC powders, our focus turned on the main goal of the study; that of designing variable material substrates to improve antenna performance and more specifically bandwidth. To do so, we extended the SIMP (design) method along with the SLP optimization method to achieve a pre-specified bandwidth for a fixed size patch antenna. Critical to the design process was the sensitivity analysis and the use of fast and general analysis tools. For a specific patch antenna example, a nonuniform substrate (mix of $\varepsilon_r = 100$ and $\varepsilon_r = 1$) was designed and shown to yield a 250% bandwidth increase. This is a substantial improvement given that the starting point of the design was based on a

highly mismatched configuration. The mismatched configuration could be further improved by incorporating the matching circuit into the design cycle. In fact, as demonstrated by the design example, by virtue of the generality and efficiency of the proposed method, there is great potential for assuming any degree of design freedom to improve RF devices performance. The design is finally filtered and solidified to achieve a manufacturable design with retained improved performance. The fabricated final design using TGM demonstrates the ability to design and manufacture novel material compositions for dramatically new applications in a practical way.

ACKNOWLEDGMENT

The authors would like to acknowledge the material characterization and fabrication efforts by A. Knapp and Dr. Y. Koh under the supervision of Prof. Dr. J. Halloran at the Material Science and Engineering Department at the University of Michigan.

REFERENCES

[1] C. A. Kyriazidiou, R. E. Diaz, and N. G. Alexopoulos, "Novel material with narrow-band transparency window in the bulk," *IEEE Trans. Antennas Propagat.*, vol. 48, pp. 107–116, Jan. 2000.

[2] D. R. Smith, D. C. Vier, N. Kroll, and S. Schultz, "Direct calculation of permeability and permittivity for a left-handed metamaterial," *Appl. Phys. Lett.*, vol. 77, no. 14, pp. 2246–2248, Oct. 2000.

[3] F. Yang and Y. Rahmat-Samii, "A low profile circularly polarized curl antenna over electromagnetic band-gap (EBG) surface," *Microw. Opt. Tech. Lett.*, vol. 31, no. 4, pp. 264–267, Nov. 2001.

[4] J. M. Johnson and Y. Rahmat-Samii, "Genetic algorithms and method of moments (GA/MoM) for the design of integrated antennas," *IEEE Trans. Antennas Propagat.*, vol. 47, pp. 1606–1614, Oct. 1999.

[5] E. Michielssen, J. M. Sajer, S. Ranjithan, and R. Mittra, "Design of light-weight, broad-band microwave absorbers using genetic algorithms," *IEEE Trans. Microwave Theory Tech.*, vol. 41, pp. 1024–1031, June/July 1993.

[6] Z. Li, Y. E. Erdemli, J. L. Volakis, and P. Y. Papalambros, "Design optimization of conformal antennas by integrating stochastic algorithms with the hybrid finite-element method," *IEEE Trans. Antennas Propagat.*, vol. 50, pp. 676–684, May 2002.

[7] D. S. Weile, E. Michielssen, and D. E. Goldberg, "Genetic algorithm design of Pareto optimal broadband microwave absorbers," *IEEE Trans. Electromagn. Compat.*, vol. 38, pp. 518–525, 1996.

[8] M. P. Bendsøe and N. Kikuchi, "Generating optimal topologies in structural design using a homogenization method," *Comput. Methods Appl. Mechan. Eng.*, vol. 71, pp. 197–224, 1988.

[9] O. Sigmund and S. Torquato, "Design of materials with extreme thermal expansion using a three-phase topology optimization method," *J. Mech. Phys. Solids*, vol. 45, no. 6, pp. 1037–1067, 1997.

[10] E. C. Silva, J. S. O. Fonseca, and N. Kikuchi, "Optimal design of periodic piezocomposites," *Comput. Methods Appl. Mechan. Eng.*, vol. 159, no. 1-2, pp. 49–77, 1998.

[11] C. Bloembaum, "The use of structural optimization in automotive design-state of the art vision," in *Proc. Int. Soc. Structural and Multidisciplinary Optimization, The World Congress of Structural and Multidisciplinary Optimization*, Buffalo, 1999, pp. 200–202.

[12] D. N. Dyck and D. A. Lowther, "Automated design of magnetic devices by optimizing material distributions," *IEEE Trans. Magn.*, vol. 32, pp. 1188–1192, May 1996.

[13] S. H. E. Choi and D. A. Lowther, "Determining boundary shapes from the optimized material distribution," *IEEE Trans. Magn.*, vol. 34, pp. 2833–2836, Sept. 1998.

[14] T. F. Eibert and J. L. Volakis, "Fast spectral domain algorithm for hybrid finite element/boundary integral modeling of doubly periodic structures," *Proc. IEEE: Microwaves, Antennas and Propagation*, vol. 147, pp. 329–334, Oct. 2000.

[15] M. P. Bendsøe, "Optimal shape design as a material distribution problem," *Structural Optimization*, vol. 1, pp. 193–202, 1989.

[16] S. S. Rao, *Engineering Optimization: Theory and Practice*, 3rd ed. New York: Wiley, 1996.

[17] H. C. Gea, "Topology optimization: A new microstructure-based design domain method," *Comput. Structures*, vol. 61, no. 5, pp. 781–788, 1996.

[18] M. Mullenborn, M. Heschel, U. D. Larsen, H. Dirac, and S. Bouwstra, "Laser direct etching of silicon on oxide for rapid prototyping," *J. Micromech. Microeng.*, vol. 6, pp. 49–51, 1996.

[19] B. C. Chen, "Optimal design of material microstructures and optimization of structural topology for design-dependent loads," Ph.D. dissertation, Univ. Michigan, Mech. Eng. Dept., 2000.

[20] K. R. Carver and J. W. Mink, "Microstrip antenna technology," *IEEE Trans. Antennas Propagat.*, vol. 29, no. 1, pp. 2–24, Jan. 1981.

[21] H. F. Lee and W. Chen, *Advances in Microstrip and Printed Antennas*. New York: Wiley, 1997.

[22] E. O. Hammerstad, "Equations for microstrip circuit design," in *Proc. 5th Eur. Microwave Conf.*, Hamburg, 1975, pp. 268–272.

[23] C. Reilly, W. J. Chappell, J. Halloran, K. Sarabandi, J. Volakis, N. Kikuchi, and L. P. B. Katehi, "New fabrication technology for ceramic metamaterials," in *IEEE Antennas and Propagation Society International Symposium*, vol. 2, San Antonio, TX, 2002, pp. 376–379.

[24] C. Fleury, "CONLIN: An efficient dual optimizer based on convex approximation concepts," *Structural Optimization*, vol. 1, pp. 81–89, 1989.

[25] R. Hanson and K. Hiebert, "A Sparse Linear Programming Subprogram," Sandia Nat. Laboratories, SAND81–0297, 1981.

[26] K. Svanberg, "The method of moving asymptotes- A new method for structural optimization," *Int. J. Numerical Methods Eng.*, vol. 24, pp. 359–373, 1987.

[27] D. N. Dyck, D. A. Lowther, and E. M. Freeman, "A Method of Computing the Sensitivity in Electromagnetic Quantities to Changes in Materials and Sources," *Int. J. Numerical Methods Eng.*, vol. 30, no. 5, pp. 3415–3418, Sept. 1994.

[28] J-F Zurcher and F. E. Gardiol, *Broadband Patch Antennas*. Norwood, MA: Artech House, 1995.

[29] O. Sigmund, "Design of multi-physics actuators using topology optimization—Part I: One material structures," *Comput. Methods Appl. Mech. Eng.*, vol. 190, pp. 6577–6604, 2001.

Gullu Kiziltas (S'00) was born in Ankara, Turkey, on December 20, 1972. She received the B.S. and M.S. degrees in mechanical engineering from the Middle East Technical University, Ankara, Turkey, in 1995 and 1998, respectively. She is currently working toward the Ph.D. degree in mechanical engineering at the University of Michigan, Ann Arbor.

From 1995 to 1998, she was a graduate student Research Assistant in the Design and Manufacturing Division at Middle East Technical University. Since September 1998, she has been a joint member of the Computational Mechanics and Radiation Laboratories (Electrical Engineering and Computer Science Department) at the University of Michigan. Her main research interests are FEM, topology optimization of antennas and filters and the design, development and fabrication of metamaterials.

Dimitris Psychoudakis (S'00) was born in Thessaloniki, Greece, on April 2,1973. He received the B.Sc. degree in physics and the M.Sc. degree in radiocommunications from the Aristotle University of Thessaloniki, in 1995 and 1999, respectively. He is currently working toward the Ph.D. degree at the Radiation Laboratory, Department of Electrical Engineering and Computer Science, University of Michigan, Ann Arbor.

His research interests include theoretical aspect of ultrasound imaging, computational electromagnetics and antenna design.

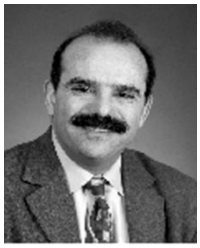

John L. Volakis (S'77–M'82–SM'89–F'96) was born on May 13, 1956, in Chios, Greece. He received the B.E. degree (*summa cum laude*) in 1978 from Youngstown State University, Youngstown, Ohio, in 1978, and the M.Sc. and Ph.D. degrees from the Ohio State University, Columbus, in 1979 and 1982, respectively.

From 1982–1984, he was with Rockwell International, Aircraft Division, Lakewood, CA, and during 1978–1982, he was a Graduate Research Associate at the Ohio State University ElectroScience Laboratory. Since 1984, he has been a Professor in the Electrical Engineering and Computer Science Department, University of Michigan, Ann Arbor. He also served as the Director of the Radiation Laboratory from 1998 to 2000. Since January 2003, he has been the Roy and Lois Chope Chair Professor of Engineering at the Ohio State University and also serves as the Director of the ElectroScience Laboratory. He has published over 200 articles in major refereed journal articles (nine of these have appeared in reprint volumes), more than 240 conference papers and nine book chapters. In addition, he coauthored two books: *Approximate Boundary Conditions in Electromagnetics* (London, U.K.: Institution of Electrical Engineers, 1995) and *Finite Element Method for Electromagnetics* (New York: IEEE Press, 1998). His primary research deals with the design of new RF materials, electromagnetic compatibility and interference, computational methods, multiphysics engineering and bioelectromagnetics.

Dr. Volakis is a Member of Sigma Xi, Tau Beta Pi, Phi Kappa Phi, and Commission B of the International Scientific Radio Union (URSI). He received the University of Michigan College of Engineering Research Excellence Award in 1998 and in the Department of Electrical Engineering and Computer Science Service Excellence Award in 2001. He served as an Associate Editor of the IEEE TRANSACTIONS ON ANTENNAS AND PROPAGATION from 1988–1992; as an Associate Editor of *Radio Science* from 1994–1997; chaired the 1993 IEEE Antennas and Propagation Society Symposium and Radio Science Meeting, and was a member of the AdCom for the IEEE Antennas and Propagation Society (1995–1998). He now serves as associate editor for the *J. Electromagnetic Waves and Applications* and the IEEE ANTENNAS AND PROPAGATION SOCIETY MAGAZINE, and the URSI Bulletin. He is also listed in several Who's Who directories, including *Who's Who in America*.

Noboru Kikuchi was born in Japan on February 4, 1951. He received the B.S. degree in civil engineering from the Tokyo Institute of Technology, Tokyo, Japan, in 1974, and the M.S. and Ph.D. degrees in aerospace engineering and engineering mechanics from the University of Texas, Austin, in 1975 and 1977, respectively.

From 1979 to 1980, he was an Assistant Professor at the Department of Aerospace Engineering and Engineering Mechanics, University of Texas. Since 1980, he has been a Professor at the Department of Mechanical Engineering, University of Michigan, Ann Arbor. He has published more than 150 papers and many textbooks and monographs. He also gave more than ten invited lectures in conferences, universities and industries per year for the past decade.

His research interests include adaptive finite element method, nonlinear problems in mechanical engineering and applied mechanics, developing micromechanical models for surface unilateral contact friction, analysis and simulation of metal and sheet forming processes, topology and general layout optimization using the homogenization design method, the homogenization method in mechanics of composites including various biomechanical materials and design of piezoceramic microstructure, as well as piezoelectric actuators.